Concentration dependence of optical phonons in the TiO_2-SnO_2 system

T. Hirata, K. Ishioka, M. Kitajima, and H. Doi
National Research Institute for Metals, 1-2-1, Sengen, Tsukuba, Ibaraki 305, Japan
(Received 17 August 1995)

The concentration dependence of optical phonons in the TiO_2-SnO_2 system whose phase diagram exhibits a miscibility gap, has been studied by Raman scattering and Fourier-transform infrared spectroscopy. X-ray diffraction confirmed that the mixed oxides $Ti_{1-x}Sn_xO_2$ with intervals $x=0.1$ are a single uniform phase (tetragonal) except some x's; no phase separation by spinodal decomposition could be avoided for $x=0.3$, 0.4, 0.5, and 0.6, characterizing x-ray-diffraction profiles by sidebands. The 449 cm^{-1} A_{1g} and 610 cm^{-1} E_g Raman modes for TiO_2 never changed linearly in frequency and linewidth with x. It is stressed that the x dependence of optical phonons is predominated by the octahedral distortion in $Ti_{1-x}Sn_xO_2$, where different/anisotropic compressibilities and thermal expansivities of each end member play a crucial role. Infrared-reflectance spectra consisting of the infrared-active A_{2u} and E_u modes between 50–900 cm^{-1}, also changed systematically with x in $Ti_{1-x}Sn_xO_2$. The concentration dependence of optical phonons in $Ti_{1-x}Sn_xO_2$ is discussed, from the viewpoint of the mode behavior of mixed crystals.

I. INTRODUCTION

Both oxides TiO_2 and SnO_2 belong to the same crystal symmetry (tetragonal) with the space group D_{4h}^{14} ($P4_2/mnm$) and two molecular units per primitive unit cell ($Z=2$). Only lattice parameters are slightly different [$a=4.732$ Å and $c=3.1871$ Å for SnO_2;[1] $a=4.594$ Å and $c=2.956$ Å for TiO_2 (Ref. 2)], because of different ionic radii ($Sn^{4+}=0.71$ Å; $Ti^{4+}=0.68$ Å).[3] The isostructure of both oxides but different lattice parameters provides the TiO_2-SnO_2 phase diagram, exhibiting a miscibility gap with a critical temperature $T_c=1430$ °C at about 50 mol % TiO_2.[4,5]

We have measured the infrared and Raman spectra of $Ti_{1-x}Zr_xO_2$, in order to investigate the concentration dependence of optical phonons in the TiO_2-ZrO_2 system.[6] However, the Zr substitution in TiO_2 was restricted to a low level since the second phase $(ZrTi)_{0.5}O_2$ (orthorhombic) emerges for $x\geqslant 0.1$ in $Ti_{1-x}Zr_xO_2$. No doubt, it is important to study with the mixed oxides over a wide concentration region, in which metal cations are replaced by any others with different radius and/or charge. The concentration dependence of optical phonons sheds light on the change in bond distances/angles or force constants. In this context, the TiO_2-SnO_2 system is rather appealing because the substitutional solid solution $Ti_{1-x}Sn_xO_2$ is formed between $0\leqslant x\leqslant 1$.

Factor-group analysis predicts the following optical phonons at the wave vector $k=0$ for tetragonal SnO_2 and TiO_2 with D_{4h}^{14}:[7,8]

$$\Gamma = A_{1g}(R)+A_{2g}+A_{2u}(\mathrm{IR})+B_{1g}(R)+B_{2g}(R)+2B_{1u} + E_g(R)+3E_u(\mathrm{IR}).$$

The three modes A_{2g} and $2B_{1u}$ are neither Raman active nor infrared active; the modes of symmetry A_{2u} and E_u are infrared active whereas the remaining A_{1g}, B_{1g}, B_{2g}, and E_g modes are Raman active. We could expect that the Raman and infrared spectra of SnO_2 and TiO_2 are similar to each other because of their isostructure (rutile type), and that these spectra of $Ti_{1-x}Sn_xO_2$ would show any concentration dependence.

The objective of the present work is to investigate the concentration dependence of the Raman- and infrared-active modes for $Ti_{1-x}Sn_xO_2$ ($0\leqslant x\leqslant 1$). A few models have been proposed to account for the mode behavior in mixed crystals.[9] Infrared-reflectance spectra of $Zr_{1-x}Hf_xO_2$ ($0\leqslant x\leqslant 1$) were measured,[10] and it is concluded that the concentration dependence of the infrared-active modes with respect to frequency, linewidth, and intensity can be reconciled with two-mode behavior. It is another issue of interest to understand the concentration dependence of optical phonons in the TiO_2-SnO_2 system from the viewpoint of the mode behavior of mixed crystals.

II. EXPERIMENT

Mixed oxides of $Ti_{1-x}Sn_xO_2$ ($0<x<1$) were prepared from TiO_2 and SnO_2 by the solid-state reaction technique. Both end member oxides (99.99%) were weighed out so as to give x's with intervals $x=0.1$ in $Ti_{1-x}Sn_xO_2$, and blended thoroughly in a mortar. Subsequently, the mixture was subjected to cold isostatic pressing at 1500 kg/cm^2 and precalcined several times in air at 1450 °C for 7 h to ensure homogeneity. Final sintering was carried out in air at 1500 °C for 5 h and followed by rapid cooling to room temperature (RT); the resultant products were cut into pellets with approximately 10 mm ϕ and 1 mm in thickness by a diamond saw, and they were used for x-ray diffraction, Fourier-transform infrared spectroscopy, and Raman scattering.

X-ray-diffraction profiles were recorded at RT by an x-ray diffractometer (Rigaku Rint2500) with Cu $K\alpha$. Lattice parameters were determined by an iterative least-squares procedure, using at least seven Bragg reflections with 2θ values in the range 25–70°. Infrared-reflectance spectra were measured in the wave-number region 50–4000 cm^{-1}, by a Fourier-transform infrared spectrometer (JEOR JIR100). Resolution was 2 cm^{-1} in the far-infrared region 50–550

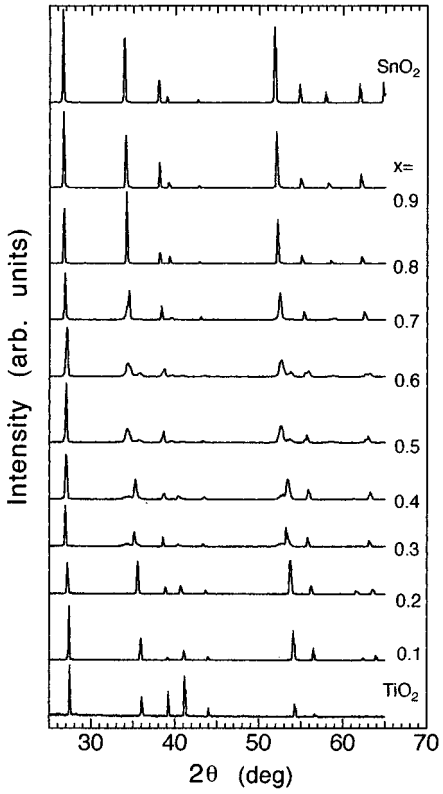

FIG. 1. The x-ray-diffraction profiles of $Ti_{1-x}Sn_xO_2$ with various x's and the end member oxides TiO_2 and SnO_2, for comparison.

cm^{-1} and 4 cm^{-1} in the mid-infrared region 400–4000 cm^{-1}. A different beam splitter, KBr or Mylar, was used with a detector of triglycine sulfate for each infrared region; a mirror of aluminum-evaporated thin film was used as the reference, to express the infrared-reflectance spectra as the sample to reference intensity ratio. Raman scattering was performed by a double monochrometer (JASCO TRS660) with a spectrometric multichannel analyzer (Princeton Inc. DRS700); the 514.5 nm Ar^+ laser was used for an exciting source with approximately 20 mW power, and all Raman spectra were recorded at RT in a backscattering geometry.

III. RESULTS

A. Lattice parameters

Figure 1 shows the x-ray-diffraction profiles of $Ti_{1-x}Sn_xO_2$ with various x's and the end members TiO_2 and SnO_2, for comparison. It is evident that all Bragg reflections assigned to tetragonal TiO_2 shift to lower 2θ values with increasing x in $Ti_{1-x}Sn_xO_2$, indicating the lattice expansion; this is evidenced by a down shift of the (211) reflection at about $2\theta=54°$ for TiO_2, for example. In addition, it should be noted that the x-ray-diffraction profiles for $x=0.3$, 0.4, 0.5, and 0.6 reveal the sidebands flanked with Bragg reflections that belong to the tetragonal unit cell.

Figure 2 depicts an example of x-ray-diffraction profile of $Ti_{1-x}Sn_xO_2$ with $x=0.6$, where the sideband is flanked with the (211) reflection at about $2\theta=54°$. It is most probable that this extra peak is originated from the phase separation by spinodal decomposition in the TiO_2-SnO_2 system.[11,12] In general, thermodynamically unstable solutions phase separated

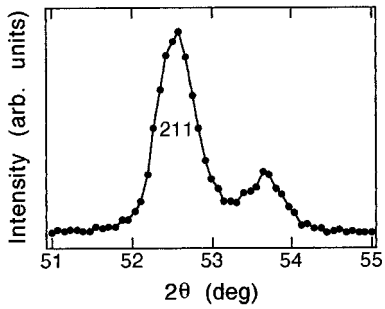

FIG. 2. The x-ray-diffraction profile of $Ti_{1-x}Sn_xO_2$ with $x=0.6$ between $2\theta=51$–55°, to demonstrate a sideband flanked with the (211) Bragg reflection that belongs to the tetragonal unit cell; this sideband is originated from the phase separation by spinodal decomposition.

by spinodal decomposition and the sidebands are observed in x-ray-diffraction profiles as shown in Fig. 2; we notice that no rapid cooling from 1500 °C to RT was sufficient to prevent the decomposition of $Ti_{1-x}Sn_xO_2$ with a few x's into a two-phase system.

In Fig. 3, the lattice parameters a and c are plotted as a function of x for $Ti_{1-x}Sn_xO_2$; the axial ratio c/a (tetragonality) and the unit-cell volume $V=a^2c$ are shown as well. The lattice parameters of TiO_2 and SnO_2 coincide with the previous data.[2,3] However, it seems difficult to connect the lattice parameters of each end member by a linear relationship, even if the errors in c and a (no more than 0.5%) are taken into consideration. Rather, there are some deviations from Vegard's law. In fact, it has been found that there are positive deviations from Vegard's law in the TiO_2-SnO_2 system, which can be predicted using a theory based on nonlinear second-order elasticity.[4]

It is evident that the data for $x=0.3$, 0.4, 0.5, and 0.6 are responsible for the noticeable deviations from Vegard's law. It is likely that the phase separation by spinodal decomposition affects the lattice paraemters at these x's. The axial ratio c/a also exhibits anomalies over the concentration region $x=0.3$–0.6 reflecting the scattered lattice parameters at these x's.

The unit-cell volume of $Ti_{1-x}Sn_xO_2$ increases monotonously with x. The monotonous increase of V indicates that the lattice of $Ti_{1-x}Sn_xO_2$ would relax as Sn^{4+} with a larger ionic radius is substituted for Ti^{4+} in TiO_2.

B. Infrared-reflectance spectra

Figure 4 displays the infrared-reflectance spectra of $Ti_{1-x}Sn_xO_2$ in the two wave-number regions that partly overlap. The infrared-reflectance spectrum of TiO_2, which is characterized by the two E_u modes at 398/516 cm^{-1} and the A_{2u} mode (broad) over 200–300 cm^{-1}, is in close agreement with the literature;[13–16] the remaining E_u mode coexists with the A_{2u} mode over 200–300 cm^{-1}. Numerous spiky features over 50–300 cm^{-1} are due to water vapor and a sharp band at 668 cm^{-1} is attributed to CO_2 in ambient atmosphere. As for the infrared-reflectance spectrum of SnO_2 which is comparable to the literature,[8] a small band around 450 cm^{-1} is identified with the A_{2u} mode. A hump at about 600 cm^{-1} can be assigned to the infrared-active mode of E_u symmetry. The

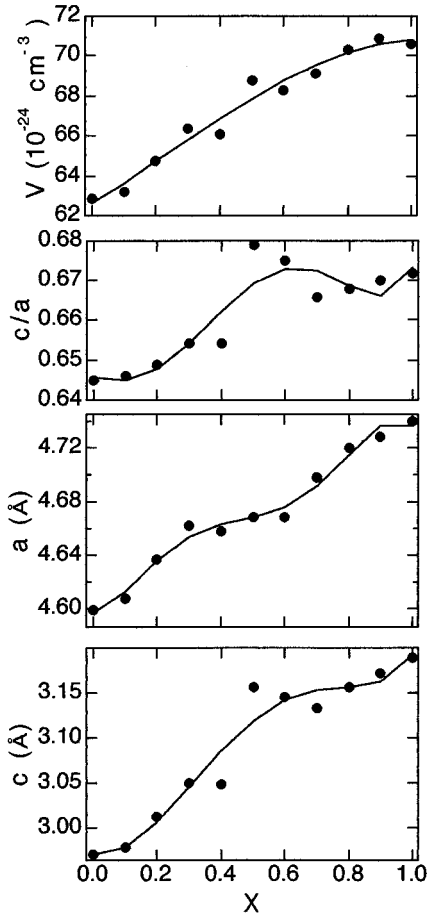

FIG. 3. The lattice parameters a and c as a function of x for $Ti_{1-x}Sn_xO_2$; the axial ratio c/a (tetragonality) and the unit-cell volume $V=a^2c$ are shown as well; note that the lines connecting data points are only a guide to eyes, and the errors in a and c (no more than 0.5%) approximately correspond to three times the size of symbols.

polarized infrared-reflectance spectra of single SnO_2 crystals allow to reveal the A_{2u} mode with the electric vector of the radiation parallel to the c axis (E_{parall}) and the three E_u modes with the electric vector perpendicular to the c axis (E_{perpend}). In fact, the imaginary part ε'' of the dielectric parameters, which were obtained from a Kramers-Kronig analysis of the polarized infrared-reflectance spectra of single SnO_2 crystals,[8] show three resonances at 244, 293, and 618 cm^{-1} for E_{perpend} and a strong resonance at 477 cm^{-1} for E_{parall}. In view of these results, it seems that the remaining two E_u modes appear around 200 and 300 cm^{-1}, respectively, in our infrared-reflectance spectrum of SnO_2 (polycrystalline).

The striking band at 770 cm^{-1} in the infrared-reflectance spectrum of SnO_2 is regarded as the longitudinal infrared mode of E_u symmetry. Another spectral feature of interest is that the two dips between the E_u modes at 516 and 398 cm^{-1}, and the 398 cm^{-1} E_u mode and the A_{2u} mode for TiO_2 become invisible and shift downwards with x in $Ti_{1-x}Sn_xO_2$. Besides, the spectral weight totally shifts to low wave numbers with increasing x since the lattice of $Ti_{1-x}Sn_xO_2$ expands with x, hence the bond strength lessens.

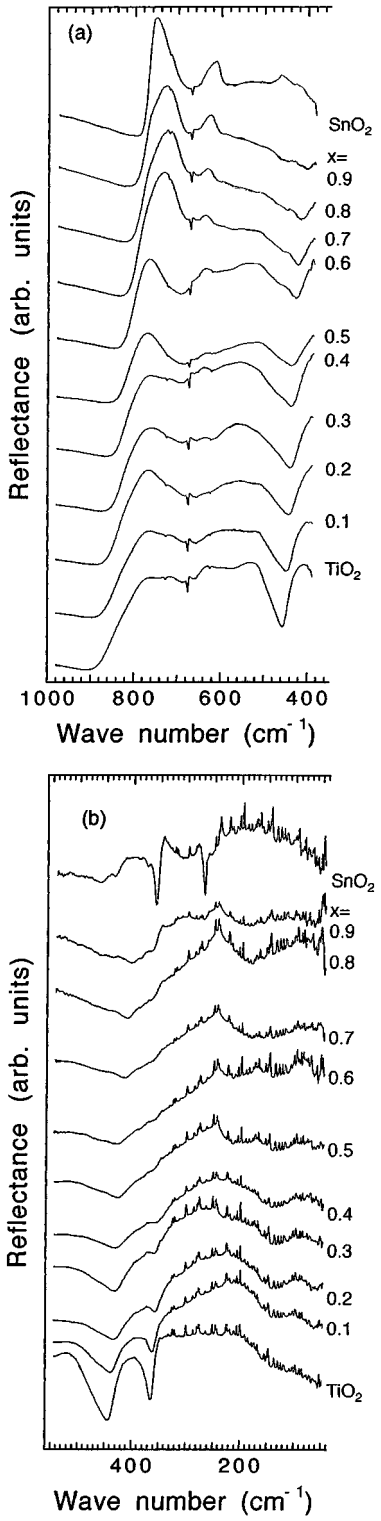

FIG. 4. The infrared-reflectance spectra of $Ti_{1-x}Sn_xO_2$ with various x's in two wave-number regions that partly overlap; 380–980 cm^{-1} (a) and 60–550 cm^{-1} (b).

No attempt has been made to extract dispersion parameters such as the oscillator strength, the damping factor and the frequency of each infrared-active mode, by a Kramers-Kronig analysis of our infrared-reflectance spectra. It might be expected that these dispersion parameters depend on x. However, the systematic spectral changes of $Ti_{1-x}Sn_xO_2$

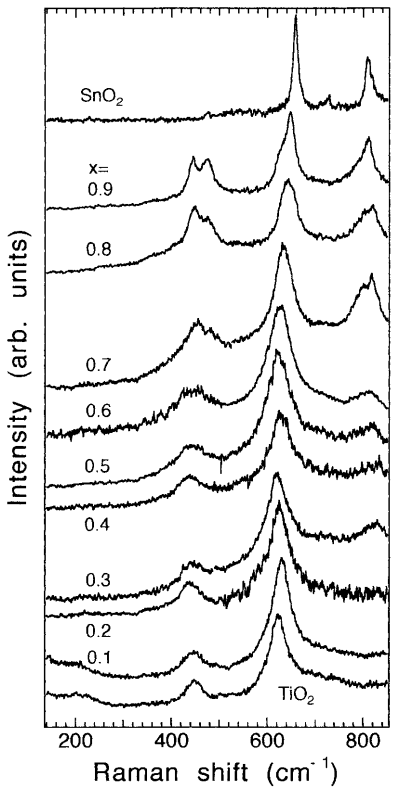

FIG. 5. The Raman spectra of $Ti_{1-x}Sn_xO_2$ with various x's in the frequency region 100–820 cm^{-1}.

with x are fairly informative concerning the concentration dependence of the infrared-active modes for $Ti_{1-x}Sn_xO_2$.

C. Raman spectra

Figure 5 shows the Raman spectra of $Ti_{1-x}Sn_xO_2$ in the frequency region 100–820 cm^{-1}. The Raman spectrum of TiO_2 agrees with the literature[13,14,17–23] except that the 143 cm^{-1} B_{1g} mode is not detected here. The broad band at 235 cm^{-1}, which is explained in terms of disorder-induced effect or second-order Raman scattering,[14,22–25] is not well resolved either; besides, the 826 cm^{-1} B_{2g} mode is invisible because of its weak intensity. In the present work, the Raman-active modes of symmetry E_g and A_{1g} are observed at 449 and 610 cm^{-1}, respectively.

On the other hand, the Raman spectrum of SnO_2 exhibits the 631 cm^{-1} A_{1g} mode and the 800 cm^{-1} B_{2g} mode, in agreement with the literature,[25–27] whereas the 123 cm^{-1} B_{1g} mode is not observed and the 475 cm^{-1} E_g mode is detected only slightly. The intensity of the B_{1g} mode $I(B_{1g})$ is too low *vis-a-vis* the A_{1g} mode intensity $I(A_{1g})$, i.e., $I(B_{1g})<10^{-3}I(A_{1g})$,[26] this makes its detection difficult. It is obvious that the Raman spectra of $Ti_{1-x}Sn_xO_2$ vary with x. The 800 cm^{-1} B_{2g} mode gets observable for $x>0.3$ and increases in intensity with x. It also appears that the 610 cm^{-1} A_{1g} mode and the 449 cm^{-1} E_g mode for TiO_2 change in frequency and linewidth with x; another striking feature is that the 420 cm^{-1} E_g mode splits for $x\geq 0.7$.

In order to demonstrate these spectral features, the Raman-active A_{1g} and E_g modes are blown up in Fig. 6. The frequency and linewidth of these modes were determined

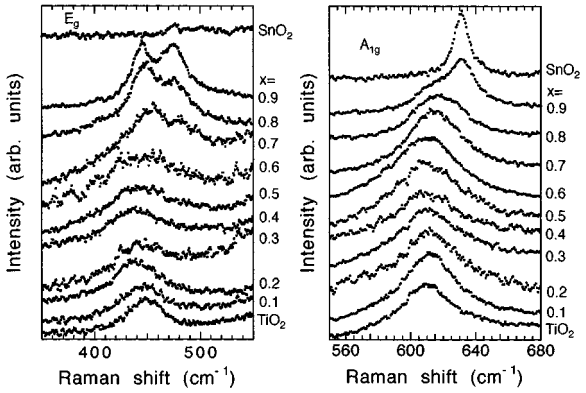

FIG. 6. Blowup of the Raman-active E_g and A_{1g} modes for $Ti_{1-x}Sn_xO_2$ with various x's.

by fitting the data to Lorenzian curve $L(\omega)=h_0+h_1/[(\omega-\omega_0)^2+\Gamma^2]$, where h_0 is the background intensity, h_1 the intensity scale factor, ω_0 is the mode frequency, and Γ is the linewidth. It should be emphasized that fitting was nicely achieved, implying that the x dependence of the Raman-active modes with respect to frequency and linewidth is of great significance.

Figure 7 shows the x dependence of frequency and linewidth for the two Raman-active modes in question. No significant change in frequency occurs up to $x=0.6$ for the A_{1g}

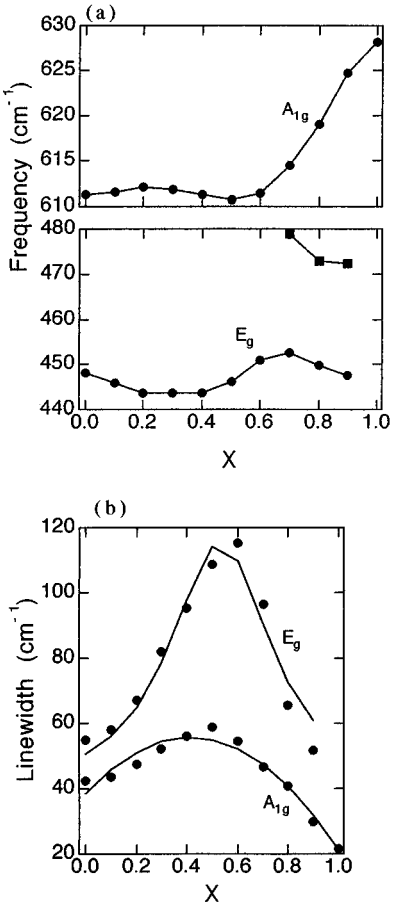

FIG. 7. The frequency (a) and linewidth (b) of the two Raman-active E_g and A_{1g} modes as a function of x for $Ti_{1-x}Sn_xO_2$.

TABLE I. Frequencies of the Raman- and infrared-active modes for SnO_2 and TiO_2. The figures in parentheses represent the frequencies of the longitudinal infrared modes. The data of the Raman- and infrared-active modes are from Refs. 23 and 8 for SnO_2, Refs. 26 and 30 for TiO_2, respectively; note the data in Refs. 30 and 15 are comparable to each other.

	B_{1g}	E_g	A_{1g}	B_{2g}	E_u	E_u	E_u	A_{2u}
SnO_2	123	475	634	776	244	293	618	477
					(276)	(366)	(770)	(705)
TiO_2	143	447	612	826	183	388	500	167
					(373)	(458)	(806)	(811)

mode, then it considerably increases toward the A_{1g} mode frequency for SnO_2 (628 cm^{-1}). On the other hand, the E_g mode somewhat softens up to $x=0.4$, whereupon it increases slightly and splits for $x \geqslant 0.7$. In Fig. 7, each frequency of the split E_g modes is plotted as well.

The linewidth of both Raman-active modes increases up to $x=0.6$, and it subsequently decreases through a maximum at about $x=0.5$; note that the linewidth of the E_g mode is represented as the sum of each linewidth of the split E_g modes for $x \geqslant 0.7$. It was remarked that the phase separation by spinodal decomposition takes place at some x's before and after $x=0.5$ (the spinodal region). Interestingly enough, the linewidth vs x curve for both Raman-active modes is similar to the phase diagram, which exhibits a miscibility gap with the maximum at about 50 mol % TiO_2 in the TiO_2-SnO_2 system.[4,5]

IV. DISCUSSION

Setting aside a question whether the x dependence of the Raman-active modes for $Ti_{1-x}Sn_xO_2$ is linear or nonlinear from the viewpoint of the mode behavior of mixed crystals, it is first surprising that the A_{1g} mode for SnO_2 shows its higher frequency as compared with TiO_2, in spite of SnO_2 being less compact than TiO_2; notice that the same situation applies to the E_g mode too. This is at variance with the conception that the bond strength lessens and optical phonons soften,[29] if the lattice becomes more loose. In accordance to this conception, the Raman-active modes of symmetries B_{1g} and B_{2g} for SnO_2 are actually softer than the corresponding modes for TiO_2.[27,28] Table I compares the frequencies of the Raman- and infrared-active modes for SnO_2 and TiO_2. It obviously depends on the Raman- and infrared-active modes whether optical phonons soften or stiffen.

Figure 8 shows the rutile structure, and atom displacements when viewing along the c axis for the Raman- and infrared-active modes in this structure. This figure demonstrates the significant role of the TiO_6 octahedron, which is a building unit of the rutile structure. Here, it should be recalled that the compressibilities κ and thermal expansivities β of SnO_2 and TiO_2 are different and anisotropic, and that the ratios $\beta_a/\beta_c(\kappa_a/\kappa_c)$ for SnO_2 are reversed from those for TiO_2,[24,26] as compiled in Table II. This implies that the structures of SnO_2 and TiO_2 deform in opposite directions with changes in either temperature or pressure. In other words, the c/a ratio decreases with increasing temperature for SnO_2 whereas it increases for TiO_2; the c/a ratio increases with

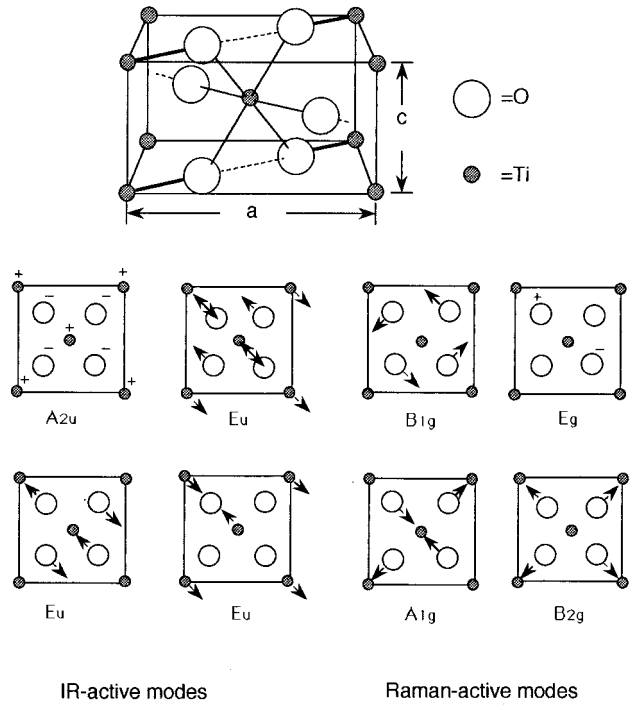

FIG. 8. Rutile structure and atom displacements when viewing along the c axis for the Raman- and infrared-active modes in this structure after Refs. 24 and 30.

increasing pressure for SnO_2 but decreases for TiO_2. Straightforwardly, this means that the ions move easily along the c axis than the a axis for TiO_2 whereas the situation is quite reverse in SnO_2. Based on these facts, it is considered that the octahedron fairly distorts so as to reproduce the reversed ratios $\beta_a/\beta_c(\kappa_a/\kappa_c)$ between SnO_2 and TiO_2, as Sn is substituted for Ti to form $Ti_{1-x}Sn_xO_2$. We would incline to regard that the octahedral distortion of TiO_6 is closely related to either softening or stiffening of the Raman- and infrared-active modes in $Ti_{1-x}Sn_xO_2$.

The bulk modulus of the octahedron is given by $K_{\mathrm{octa}}=7.5S^2Z_cZ_a/\langle d\rangle^3$, where Z_c and Z_a are cation and anion formal charge, $\langle d\rangle$ is the mean cation-anion bond distance, and S^2 is an empirical ionicity term equal to 0.5 for oxides.[31] The data of the bond distances[31] yield 4.0 and 4.9

TABLE II. Compressibilities $\kappa_{a,c}$ and thermal expansivities $\beta_{a,c}$ of SnO_2 and TiO_2 after Ref. 26; the ratios $\kappa_a/\kappa_c(\beta_a/\beta_c)$ are given as well. The volume expansion (compressibility) is equal to $\beta_v(\kappa_v)=2\beta_a(2\kappa_a)+\beta_c(k_c)$. $\kappa_{a,c}$: $T=296$ K; $\beta_{a,c}$: $T>350$ K.

	SnO_2 [a]	TiO_2 [a]
κ_a (10^{-4}/kbar)	1.3	1.93
κ_c (10^{-4}/kbar)	1.9	0.8
κ_a/κ_c	0.68	2.41
β_a (10^{-6}/K)	4.0	8.5
β_c (10^{-6}/K)	3.7	11.0
β_a/β_c	1.08	0.77
κ_v (10^{-4}/kbar)	4.5	4.73
β_v (10^{-6}/K)	11.0	28.0

[a]Reference 26.

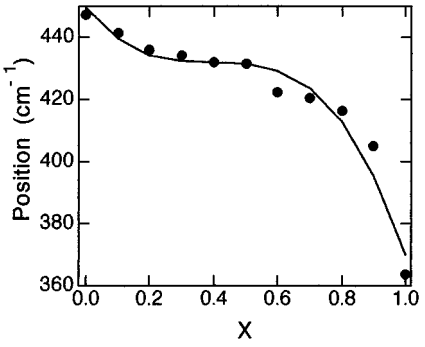

FIG. 9. The dip's position ($\sim$450 cm^{-1} for TiO_2) between the two E_u modes in the infrared-reflectance spectra of $Ti_{1-x}Sn_xO_2$ is plotted as a function of x.

as K_{octa}'s of TiO_2 and SnO_2, respectively. This indicates that the octahedron of SnO_6 is stiffer than TiO_6, which may account for the higher frequency of some optical phonons for SnO_2 in reference to TiO_2.

However, the change in the six-bond distances and/or bond angles for TiO_6 with x in $Ti_{1-x}Sn_xO_2$ is anisotropic or complex, reflecting the reversed ratios $\beta_a/\beta_c(\kappa_a/\kappa_c)$ between SnO_2 and TiO_2 such that either softening or stiffening of optical phonons can be induced. Simply from a mass change of the metal-O bonds upon substitution, optical phonons are expected to soften because the frequency $\nu(x)$ is given by $\nu(x)=[f(x)/\mu(x)]^{1/2}$, where $f(x)$ is the force constant, $\mu(x)$ is the reduced mass defined by $\mu(x)^{-1}=(1-x)/m_{\text{Ti}}+x/m_{\text{Sn}}$; note $m_{\text{Ti}}<m_{\text{Sn}}$ with $m_{\text{Ti(Sn)}}$ being the atomic mass of Ti or Sn.

As for the x dependence of the infrared-active modes for $Ti_{1-x}Sn_xO_2$, the dip's position ($\sim$450 cm^{-1} for TiO_2) between the two E_u modes is plotted as a function of x in Fig. 9. It can be seen that the dip's position changes only slightly up to $x=0.6$, whereupon its significant reduction follows exhibiting a clear nonlinear dependence; the positional change of this dip can be regarded as the E_u mode shift in frequency with x.

As far as we are concerned with Figs. 7 and 9, the x dependence of optical phonons in the TiO_2-SnO_2 system is not linear with respect to frequency or linewidth, ruling out one-mode behavior, in which we should predict a linear relationship between the mode frequencies of each end member. In the random-element-isodisplacement models,[32–36] it is assumed that the three force constants $f_{ij}(x)$ in a mixed crystal $AB_{1-x}C_x$ $(ij=AB,AC,BC)$ have the same compositional dependence such that $f_{ij}(x)=f_{ij}(0)[1+\Theta x]$, where $f_{ij}(0)$ is the force constant at $x=0$ and Θ is a constant which describes the effect of lattice parameter change on the force constants. The lattice parameters change nonlinearly with x for $Ti_{1-x}Sn_xO_2$, supporting positive deviations from Vegard's law in the TiO_2-SnO_2 system.[4] This urges us to consider that the constant Θ depends on x,[36,37] and consequently the nonlinear x dependence of optical phonons is predicted through the x-dependent constant Θ, ruling out one-mode behavior for $Ti_{1-x}Sn_xO_2$; we have already commented that the nonlinear change in lattice parameters is due to the phase separation by spinodal decomposition.

Finally, we must give any probable cause for splitting of the E_g mode for $x\geqslant 0.7$. Inspection of Fig. 6 reveals that the 470 cm^{-1} mode of the split E_g modes corresponds to the E_g mode for SnO_2 (subtly visible) in Fig. 6. This assures that TiO_2- and SnO_2-rich phases, which may exist microscopically in $Ti_{1-x}Sn_xO_2$ with higher x's, can be detected by Raman scattering.

V. CONCLUSIONS

The concentration dependence of optical phonons in the TiO_2-SnO_2 system has been studied by Raman scattering and Fourier-transform infrared spectroscopy. The 610 cm^{-1} A_{1g} mode and the 449 cm^{-1} E_g mode for TiO_2 exhibited a nonlinear x dependence with respect to frequency and linewidth. It is stressed that the octahedral distortion of TiO_6 predominates the x dependence of optical phonons in $Ti_{1-x}Sn_xO_2$, whose end members deform in opposite directions with changes in either pressure or temperature because of their different/anisotropic compressibilities and thermal expansivities. The infrared-reflectance spectra of $Ti_{1-x}Sn_xO_2$ also changed systematically with x. The concentration dependence of optical phonons is discussed from the viewpoint of the mode behavior of mixed crystals, ruling out one-mode behavior for $Ti_{1-x}Sn_xO_2$. It is concluded that the nonlinear x dependence of optical phonons is predicted through the x-dependent term which describes the effect of lattice parameter change on the force constants. Actually, x-ray diffraction showed the nonlinear change in lattice parameters, supporting positive deviations from Vegard's law in the TiO_2-SnO_2 system. It was also found that $Ti_{1-x}Sn_xO_2$ with some x's ($x=0.3$, 0.4, 0.5, and 0.6) could phase separate by spinodal decomposition, as evidenced by the sidebands flanked with Bragg reflections in x-ray-diffraction profiles. The present work somewhat highlights the effect of the phase separation on the x dependence of optical phonons for $Ti_{1-x}Sn_xO_2$.

[1] G. McCarthy and J. Welton, J. Powder Diffraction **4**, 156 (1989).
[2] W. H. Baur and A. A. Khan, Acta Crystallogr. B **27**, 2133 (1971).
[3] *Handbook of Chemistry and Physics*, 53rd ed., edited by R. C. Weast (Chemical Rubber, Cleveland, 1972–1973).
[4] M. Park, T. E. Mitchell, and A. H. Heuer, J. Am. Ceram. Soc. **58**, 43 (1975).
[5] D. Garcia and D. Speidel, J. Am. Ceram. Soc. **53**, 322 (1972).
[6] T. Hirata, M. Kitajima, K. G. Nakamura, and E. Asari, J. Phys. Chem. Solids **55**, 349 (1994).
[7] V. A. Maroni, J. Phys. Chem. Solids **49**, 307 (1988).
[8] R. S. Katiyar, P. Dawson, M. M. Hargreave, and G. R. Wilkinson, J. Phys. C **4**, 2421 (1971).
[9] D. W. Taylor, in *Optical Properties of Mixed Crystals*, edited by R. J. Elliot and I. P. Ipatova (Elsevier Science, Amsterdam, 1988), p. 35.
[10] T. Hirata, Phys. Rev. B **50**, 2874 (1994).
[11] V. S. Stubican and A. H. Schultz, J. Am. Ceram. Soc. **53**, 211 (1970).

[12] P. K. Gupta and A. R. Cooper, Philos. Mag. **21**, 611 (1970).
[13] M. Ocana, J. V. Garcia-Ramos, and C. J. Serna, J. Am. Ceram. Soc. **75**, 2010 (1972).
[14] M. Ocana, V. Fornes, J. V. Garcia Ramos, and C. J. Serna, J. Solid State Chem. **75**, 364 (1988).
[15] F. Gervais and B. Piriou, Phys. Rev. B **10**, 1642 (1974).
[16] W. G. Spitzer, R. C. Miller, D. A. Kleinman, and L. E. Howarth, Phys. Rev. **126**, 1710 (1962).
[17] U. Balachandran and N. G. Eror, J. Solid State Chem. **42**, 276 (1982).
[18] J. F. Mammone, S. K. Sharma, and M. Nicol, Solid State Commun. **34**, 799 (1980).
[19] Y. Hara and M. Nicol, Phys. Status Solidi B **94**, 317 (1979).
[20] H. Arashi, J. Phys. Chem. Solids **53**, 355 (1992).
[21] J. F. Mammone, N. Nicol, and S. K. Sharma, J. Phys. Chem. Solids **42**, 379 (1981).
[22] R. J. Betsch, H. L. Park, and W. B. White, Mater. Res. Bull. **26**, 613 (1991).
[23] S. P. S. Porto, P. A. Fleury, and T. C. Damen, Phys. Rev. B **154**, 522 (1967).
[24] G. A. Samara and P. S. Peercy, Phys. Rev. B **7**, 1131 (1973).
[25] U. Balachandran and N. G. Eror, J. Solid State Chem. **42**, 276 (1982).
[26] P. S. Peercy and B. Morosin, Phys. Rev. B **7**, 2779 (1973).
[27] J. F. Scott, J. Chem. Phys. **53**, 852 (1970).
[28] Y. S. Hung and Fred H. Pollak, Solid State Commun. **43**, 921 (1982).
[29] I. L. Botto, E. J. Baran, C. Cascales, I. Rasines, and R. Saez Puche, J. Phys. Chem. Solids **52**, 431 (1991).
[30] D. M. Eagles, J. Phys. Chem. Solids **25**, 1243 (1964).
[31] R. M. Hazen and L. W. Finger, J. Phys. Chem. Solids **42**, 143 (1981).
[32] Y. S. Chen, W. Shockley, and G. L. Pearson, Phys. Rev. **151**, 648 (1966).
[33] M. Ilegems and G. L. Pearson, Phys. Rev. B **1**, 1576 (1970).
[34] G. Lucovsky, K. Y. Cheng, and G. L. Pearson, Phys. Rev. B **12**, 4135 (1975).
[35] G. Lucovsky, R. D. Burnham, and A. S. Alimonda, Phys. Rev. B **14**, 2503 (1976).
[36] D. L. Peterson, A. Petrou, W. Giriat, A. K. Ramdas, and S. Rodriguez, Phys. Rev. B **33**, 1160 (1986).
[37] P. D. Lao, Yile Guo, G. G. Siu, and S. C. Shen, Phys. Rev. B **48**, 11 701 (1993).